HHS Public Access

Author manuscript

*Mol Cancer Res*. Author manuscript; available in PMC 2018 December 01.

Published in final edited form as:

*Mol Cancer Res*. 2017 December ; 15(12): 1667–1677. doi:10.1158/1541-7786.MCR-17-0333.

# Syngeneic Mouse Models of Oral Cancer are Effectively Targeted by anti-CD44-based NIR-PIT

**Tadanobu Nagaya**[1], **Yuko Nakamura**[1], **Shuhei Okuyama**[1], **Fusa Ogata**[1], **Yasuhiro Maruoka**[1], **Peter L. Choyke**[1], **Clint Allen**[2], and **Hisataka Kobayashi**[1]

[1]Molecular Imaging Program, Center for Cancer Research, National Cancer Institute, National Institutes of Health, Bethesda, Maryland, 20892, United States of America

[2]Tumor Biology Section, Head and Neck Surgery Branch, National Institutes of Deafness and Other Communication Disorders, National Institutes of Health, Bethesda, Maryland, 20892, United States of America

## Abstract

Oral cavity squamous cell carcinoma (OSCC) is considered one of the most aggressive subtypes of cancer. Anti-CD44 monoclonal antibodies (mAbs) are a potential therapy against CD44 expressing OSCC, however, to date the therapeutic effects have been disappointing. Here, a new cancer treatment is described, near-infrared photoimmunotherapy (NIR-PIT), that uses anti-CD44 mAbs conjugated to the photoabsorber, IR700DX. This conjugate is injected into mice harboring one of three CD44 expressing syngeneic murine oral cancer cell (MOC) lines, MOC1 (immunogenic), MOC2 mKate2 (moderately immunogenic), and MOC2-luc (poorly immunogenic). Binding of the anti-CD44-IR700 conjugate was shown to be specific and cell-specific cytotoxicity was observed after exposure of the cells to NIR *in vitro*. The anti-CD44-IR700 conjugate, when assessed *in vivo*, demonstrated deposition within the tumor with a high tumor-to-background ratio. Tumor-bearing mice were separated into four cohorts: no treatment; 100μg of anti-CD44-IR700 i.v. only; NIR light exposure only; and 100μg of anti-CD44-IR700 i.v. with NIR light exposure. NIR-PIT therapy, compared with the other groups, significantly inhibited tumor growth and prolonged survival in all three cell model systems. In conclusion, these data reveal that anti-CD44 antibodies are suitable as mAb-photoabsorber conjugates for NIR-PIT in MOC cells.

## Introduction

Oral cavity squamous cell carcinoma (OSCC) is a common, aggressive, carcinogen-induced malignancy (1). Despite advances in detection and standard therapeutic approaches such surgery, chemotherapy, and radiation, the prognosis for OSCC has remained poor due to a high rate of locoregional recurrence and development of distant metastasis (1–3). Furthermore, approximately two-thirds of OSCC patients have locoregionally advanced disease at the time of diagnosis, resulting in increased morbidity following surgical ablation and adjuvant therapies (1–3). Thus, there is a need for new therapies in this disease.

Corresponding author: Hisataka Kobayashi, National Cancer Institute, Bldg. 10, RmB3B69, 10 Center Dr., MD 20892-1088. Phone: 301-435-4086; Fax: 301-402-3191; kobayash@mail.nih.gov.

Intratumoral heterogeneity has been implicated as a major cause of treatment failure. The presence of cancer stem-like cells in tumors has been proposed as one source of tumor heterogeneity as well as a cause of resistance to chemotherapy and radiation (4–8). CD44 is a well-known marker of cancer stem-like cells and mediates intercellular adhesion, cell orientation, migration, and matrix-cell signaling processes (9–11). CD44 is expressed in various types of cancer, including the majority of head and neck cancers. High expression of CD44 is associated with poor local control rates and resistance to therapy (12–14). Suppression of CD44 can lead to tumor growth delay (10, 12, 15). Thus, CD44 has become an important target for antibody-based therapies. In clinical studies a monoclonal anti-CD44 antibody demonstrated some efficacy in phase 1 studies, however, lethal toxic epidermal necrolysis halted further development (16–18).

Near infrared photoimmunotherapy (NIR-PIT) is a newly developed cancer treatment that employs a targeted monoclonal antibody (mAb)-photo-absorber conjugate (APC) (19). The antibody binds to the appropriate cell surface antigen and the photo-activatable silica-phthalocyanine dye, IRDye700DX (IR700), induces lethal damage to cell membrane after NIR-light exposure. NIR-PIT has been shown to be effective with a variety of different antibodies (19–25). Moreover, a first-in-human Phase 1 trial of NIR-PIT with an APC targeting epidermal growth factor receptor (EGFR) in patients with inoperable head and neck cancer was approved by the US Food and Drug Administration (FDA; https://clinicaltrials.gov/ct2/show/NCT02422979).

NIR-PIT induces selective immediate, immunogenic cell death (ICD) unlike conventional cancer therapies that typically induce apoptotic cell death (26). To explore the potential immune activating effects of NIR-PIT, we utilized newly established syngeneic murine oral cancer (MOC) models, consisting of MOC1 (immunogenic), MOC2 mKate2 (moderately immunogenic), and MOC2-luc (poorly immunogenic) cell lines. MOC1 cells display a high somatic gene alteration rate and generate tumors with slow primary tumor growth that do not metastasize, have high MHC class I expression, and show robust effector immune cell infiltration. Conversely, MOC2 cells have fewer genetic alterations, generate aggressive tumors that metastasize early to draining lymph nodes, have very low MHC class I expression, and demonstrate limited effector immune cell infiltration (27–29). Thus, these experiments demonstrate the range of immunologic effects of NIR-PIT in various syngeneic tumor models.

## Materials and Methods

### Reagents

Water soluble, silica-phthalocyanine derivative, IRDye 700DX NHS ester was obtained from LI-COR Biosciences (Lincoln, NE, USA). An anti-mouse/human CD44-specific mAb, IM7, was purchased from BioXCell (West Lebanon, NH, USA). All other chemicals were of reagent grade.

### Synthesis of IR700-conjugated anti-CD44 mAb

Anti-CD44 mAb (1.0 mg, 6.7 nmol) was incubated with IR700 NHS ester (65.1 μg, 33.3 nmol) in 0.1 M $Na_2HPO_4$ (pH 8.6) at room temperature for 1 h. The mixture was purified with a Sephadex G25 column (PD-10; GE Healthcare, Piscataway, NJ, USA). The protein concentration was determined with Coomassie Plus protein assay kit (Thermo Fisher Scientific Inc, Rockford, IL, USA) by measuring the absorption at 595 nm with UV-Vis (8453 Value System; Agilent Technologies, Santa Clara, CA, USA). The concentration of IR700 was measured by absorption at 689 nm to confirm the number of fluorophore molecules per mAb. The synthesis was controlled so that an average of two IR700 molecules was bound to a single antibody. We abbreviate IR700 conjugated to anti-CD44 antibody as anti-CD44-IR700. As a quality control for the conjugate, we performed sodium dodecyl sulfate-polyacrylamide gel electrophoresis (SDS-PAGE) according to previous reports (19–22). Conjugate was separated by SDS-PAGE with a 4–20% gradient polyacrylamide gel (Life Technologies, Gaithersburg, MD). A standard marker (Crystalgen Inc., Commack, NY) was used as a protein molecular weight marker. After electrophoresis at 80 V for 2.5 h, the gel was imaged with a Pearl Imager (LI-COR Biosciences, Lincoln, Nebraska, USA) using a 700 nm fluorescence channel. We used diluted anti-CD44 antibody as non-conjugated control. The gel was stained with Colloidal Blue staining to determine the molecular weight of conjugate.

### Cell culture

MOC1 cells stably expressing CD44 antigen, MOC2 cells expressing CD44 and luciferase or CD44 and mKate2 (far-red fluorescent protein TagFP635) were used in this study. We abbreviate one cell line as MOC2-luc and the other MOC2-mKate. Possessing fluorescence with excitation/emission maxima at 588 and 633 nm, mKate2 is almost 3-fold brighter than TagFP635 at physiological pH 7.5. The mKate2 protein is characterized by complete and fast chromophore maturation at 37°C with maturation half-time < 20 min. It is also more photo-stable under both wide-field and confocal illumination than other monomeric far-red proteins, (30, 31). High mKate2 expression was confirmed with 10 passages. All MOC cells were cultured in HyClone™ Iscove's Modified Dulbecco's Medium (IMDM; GE Healthcare Life sciences, South Logan, UT, USA)/HyClone™ Ham's Nutrient Mixture F12 (GE Healthcare Life sciences) at a 2:1 mixture with 5% fetal bovine serum (Life Technologies, Gaithersburg, MD, USA), 1% penicillin/streptomycin (Life Technologies), 5 ng/mL epidermal growth factor (EGF; EMD Millipore Corporation, Temecula, CA, USA), 400 ng/mL hydrocortisone (Sigma Aldrich, St Louis, MO, USA), and 5 mg/mL insulin (Sigma Aldrich) in tissue culture flasks in a humidified incubator at 37°C in an atmosphere of 95% air and 5% carbon dioxide (27, 32). Cells were maintained in culture for no more than 30 passages, authenticated by exome sequencing by others (33) and tested for mycoplasma.

### Flow cytometry

To verify *in vitro* anti-CD44-IR700 binding, fluorescence from cells after incubation with APC was measured using a flow cytometer (FACS Calibur, BD BioSciences, San Jose, CA, USA) and CellQuest software (BD BioSciences). MOC1 and MOC2-luc cells ($2 \times 10^5$) were seeded into 12 well plates and incubated for 24 h. Medium was replaced with fresh culture

medium containing 10 μg/mL of anti-CD44-IR700 and incubated for 6 h at 37°C. To validate the specific binding of the conjugated antibody, excess antibody (100 μg) was used to block 10 μg of APCs.

## Fluorescence microscopy

To detect the antigen specific localization and effect of NIR-PIT, fluorescence microscopy was performed (BX61; Olympus America, Inc., Melville, NY, USA). Ten thousand MOC1 and MOC2-luc cells were seeded on cover-glass-bottomed dishes and incubated for 24 h. anti-CD44-IR700 was then added to the culture medium at 10 μg/mL and incubated for 6 h at 37°C. After incubation, the cells were washed with phosphate buffered saline (PBS). The filter set to detect IR700 consisted of a 590–650 nm excitation filter, a 665–740 nm band pass emission filter. Transmitted light differential interference contrast (DIC) images were also acquired.

## *In vitro* NIR-PIT

The cytotoxic effects of NIR-PIT with anti-CD44-IR700 were determined by flow cytometric propidium iodide (PI) (Life Technologies) staining, which can detect compromised cell membranes. Two hundred thousand MOC1 and MOC2-luc cells were seeded into 12 well plates and incubated for 24 h. Medium was replaced with fresh culture medium containing 10 μg/ml of anti-CD44-IR700 and incubated for 6 h at 37°C. After washing with PBS, PBS was added, and cells were irradiated with a red light-emitting diode (LED), which emits light at 670–710nm wavelength (L690-66-60; Marubeni America Co., Santa Clara, CA, USA) at a power density of 50 $mW/cm^2$ as measured with an optical power meter (PM 100, Thorlabs, Newton, NJ, USA). Cells were scratched 1 h after treatment. PI was then added in the cell suspension (final 2 μg/mL) and incubated at room temperature for 30 min, followed by flow cytometry. Each value represents mean ± standard error of the mean (SEM) of five experiments.

For bioluminescence imaging (BLI), either two hundred thousand MOC2-luc cells were seeded into 12 well plates or twenty million cells were seeded onto a 10 cm dish; both were pre-incubated for 24 h. After replacing the medium with fresh culture medium containing 10 μg/mL of anti-CD44-IR700, the cells were incubated for 6 h at 37˚C in a humidified incubator. After washing with PBS, phenol-red-free culture medium was added. Then, cells were exposed with a LED or a NIR laser which emits light at a 685 to 695nm wavelength (BWF5-690-8-600-0.37; B&W TEK INC., Newark, DE, USA). The output power density in $mW/cm^2$ was measured with an optical power meter (PM 100, Thorlabs, Newton, NJ, USA). For luciferase activity, 150 μg/mL D-luciferin-containing media (Gold Biotechnology, St. Louis, MO, USA) was administered to PBS-washed cells 1 h after NIR-PIT and images were obtained on a BLI system (Photon Imager; Biospace Lab, Paris, France). Regions of interest (ROIs) were placed on each entire well, and the luciferase activity (photons/min) was then calculated using M3 Vision Software (Biospace Lab).

## Animal and tumor models

All *in vivo* procedures were conducted in compliance with the Guide for the Care and Use of Laboratory Animal Resources (1996), US National Research Council, and approved by the

local Animal Care and Use Committee. Six to eight week old female C57BL/6 mice (strain #000664) were purchased from Jackson Laboratory (Sacramento, CA, USA). The lower part of the body of the mice was shaved for irradiation and image analysis. During the procedure, mice were anesthetized with inhaled 3–5% isoflurane and/or via intraperitoneal injection of 1 mg of sodium pentobarbital (Nembutal Sodium Solution, Ovation Pharmaceuticals Inc., Deerfield, IL, USA). In order to determine tumor volume, the greatest longitudinal diameter (length) and the greatest transverse diameter (width) were measured with an external caliper. Tumor volumes were based on caliper measurements and were calculated using the following formula; tumor volume = length × width$^2$ × 0.5. Body weight was also measured. Mice were monitored daily for general health. Skin color was observed for signs of technology and general health indices, including weight loss and appetite loss, were assessed. Tumor volumes were measured three times a week until the tumor volume reached 2000 mm$^3$, whereupon the mice were euthanized with inhalation of carbon dioxide gas.

### *In vivo* fluorescence imaging

*In vivo* IR700 fluorescence images were obtained with a Pearl Imager (LI-COR Biosciences, Lincoln, Nebraska, USA) with a 700 nm fluorescence channel. A ROI was placed on the tumor and the average fluorescence intensity of IR700 signal was calculated for each ROI using a Pearl Cam Software (LICOR Biosciences). For mKate2 fluorescence imaging, a Maestro Imager (Cri, Woburn, MA, USA) with a band-pass excitation filter from 575 to 605 nm and a long-pass emission blue filter over 645 nm was used. The tunable emission filter was automatically increased in 10-nm increments from 630 to 850 nm at a constant exposure time (500 msec). The spectral fluorescence images consisted of autofluorescence spectra and spectra from mKate2, which were then unmixed from each other based on the characteristic spectral pattern of mKate2 using a Maestro software (CRi).

### *In vivo* bioluminescence imaging

For *in vivo* BLI, D-luciferin (15 mg/mL, 200 μL) was injected intraperitoneally and the mice were analyzed on a BLI system (Photon Imager) for luciferase activity. ROIs were set to include the entire tumor in order to quantify BLI. ROIs were also placed in the adjacent non-tumor region as background. Average luciferase activity of each ROI was calculated.

### *In vivo* fluorescence imaging studies

MOC1 cells (2.0 × 10$^6$) and MOC2-luc cells (1.5 × 10$^5$) were injected subcutaneously in the right dorsum of the mice. Tumors were studied after they reached volumes of approximately 50 mm$^3$. Serial dorsal fluorescence images of IR700 were obtained with a Pearl Imager using a 700 nm fluorescence channel before and 0, ½, 1, 2, 3, 4, 5, 6, 9, 12, 24, 48, 72, 96, 120, 144, and 168 hours after i.v. injection of 100 μg of anti-CD44-IR700 via the tail vein. Pearl Cam Software (LICOR Biosciences, Lincoln, NE, USA) was used for analyzing IR700 fluorescence intensities. Regions of interest (ROIs) were placed on the tumor and the adjacent non-tumor region as background (left dorsum). Average fluorescence intensity of each ROI was calculated. Target-to-background ratios (TBR; fluorescence intensities of target / fluorescence intensities of background) were also calculated (n = 10).

### *In vivo* NIR-PIT in a unilateral tumor model

MOC1 cells ($2.0 \times 10^6$) and MOC2-luc cells ($1.5 \times 10^5$) were injected subcutaneously in the right dorsum of the mice. Tumors were studied after they reached volumes of approximately 50 $mm^3$. To examine the therapeutic effect of *in vivo* NIR-PIT on both cells, tumor-bearing mice were randomized into 4 groups of at least 8 animals per group for the following treatments: (1) no treatment (control); (2) 100 μg of anti-CD44-IR700 i.v., no NIR light exposure (APC i.v. only); (3) NIR light exposure only, NIR light was administered at 50 $J/cm^2$ on day 0 and 100 $J/cm^2$ on day 1 (NIR light only); (4) 100 μg of anti-CD44-IR700 i.v., NIR light was administered at 50 $J/cm^2$ on day 0 and 100 $J/cm^2$ on day 1 (NIR-PIT). Serial IR700 fluorescence images, as well as white light images, were obtained before and after each NIR light exposure (day 0 and day 1), and day 2 using a Pearl Imager with a 700 nm fluorescence channel. BLI also obtained before NIR light exposure (day0), day 1 and day 2 using Photon Imager.

MOC2 mKate2 cells ($1.5 \times 10^5$) were injected subcutaneously in the right dorsum of the mice. Tumors were studied after they reached volumes of approximately 50 $mm^3$. To examine the therapeutic effect of *in vivo* NIR-PIT on MOC2 mKate2 cells, tumor-bearing mice were randomized into 2 groups of at least 10 animals per group for the following treatments: (1) no treatment (control); (2) 100 μg of anti-CD44-IR700 i.v., NIR light was administered at 50 $J/cm^2$ on day 0 and 100 $J/cm^2$ on day 1 (NIR-PIT). Serial IR700 fluorescence images, as well as white light images, were obtained before and after each NIR light exposure (day 0 and day 1), day 2, and day 3 using a Pearl Imager with a 700 nm fluorescence channel. The mKate2 fluorescence images also obtained before NIR light exposure (day 0), day 1, day 2, and day 3 using a Maestro Imager.

### *In vivo* NIR-PIT in bilateral tumors model

MOC1 cells ($2.0 \times 10^6$) and MOC2-luc cells ($1.5 \times 10^5$) were injected subcutaneously in both dorsa of the mice. Tumors were studied after they reached volumes of approximately 50 $mm^3$. Tumor-bearing mice were randomized into 2 groups of at least 8 animals per group for the following treatments: (1) no APC, NIR light was administered at 100 $J/cm^2$ only to the right-sided tumor on day 0; (2) 100 μg of anti-CD44-IR700 i.v., NIR light was administered at 100 $J/cm^2$ only to the right-sided tumor on one day after injection (day 0). The untreated left-sided tumor was shielded from light exposure by covering it with aluminum foil to prevent direct NIR light exposure. Serial IR700 fluorescence images, as well as white light images, were obtained before and after NIR light exposure (day 0), day 1 and day 2 using a Pearl Imager with a 700 nm fluorescence channel. BLI also obtained before NIR light exposure (day0), day 1 and day 2 using the Photon Imager.

MOC2 mKate2 cells ($1.5 \times 10^5$) were injected subcutaneously in both dorsa of the mice. Tumors were studied after they reached volumes of approximately 50 $mm^3$. Tumor-bearing mice were randomized into 2 groups of at least 8 animals per group for the following treatments: (1) no APC, NIR light was administered at 100 $J/cm^2$ only to the right-sided tumor on day 0; (2) 100 μg of anti-CD44-IR700 i.v., NIR light was administered at 100 $J/cm^2$ only to the right-sided tumor one day after injection (day 0). The untreated left-sided tumor was shielded from light exposure by covering it with aluminum foil to prevent direct

NIR light exposure. Serial IR700 fluorescence images, as well as white light images, were obtained before and after each NIR light exposure (day 0 and day 1), day 2, and day 3 using a Pearl Imager with a 700 nm fluorescence channel. The mKate2 fluorescence images were also obtained before NIR light exposure (day 0), day 1, day 2, and day 3 using a Maestro Imager.

### Histological analysis

To detect the antigen-specific micro-distribution in the tumor, fluorescence microscopy was performed. Tumor xenografts were excised from the right flank xenograft without treatment, 24 h after injection of anti-CD44-IR700 (APC i.v. only) and 24 h after NIR-PIT. Extracted tumors were frozen with optimal cutting temperature (OCT) compound (SAKURA Finetek Japan Co., Tokyo, Japan) and frozen sections (10 μm thick) were prepared. Fluorescence microscopy was performed using the BX61 microscope with the following filters: excitation wavelength 590 to 650 nm, emission wavelength 665 to 740 nm long pass for IR700 fluorescence. DIC images were also acquired. To evaluate histological changes, light microscopy study was also performed using Olympus BX61. Tumor xenografts were excised from mice without treatment, 24 h after injection of anti-CD44-IR700 (APC i.v. only) and 24 h after NIR-PIT. Tumors were also excised from mice with bilateral flank tumors (both treated right-sided tumors and untreated left-sided tumors) 24 h after NIR-PIT of the right tumor. Extracted tumors were also placed in 10% formalin and serial 10 μm slice sections were fixed on a glass slide with H&E staining.

### Statistical analysis

Data are expressed as means ± SEM from a minimum of five experiments, unless otherwise indicated. Statistical analyses were carried out using GraphPad Prism version 7 (GraphPad Software, La Jolla, CA, USA). Student's t test was used to compare the treatment effects with that of control *in vitro*. To compare intensity and TBR between MOC1 and MOC2-luc tumors at all time points and to compare tumor growth in a unilateral tumor model of MOC2 mKate2, the Mann Whitney test was used. For multiple comparisons, a one-way analysis of variance (ANOVA) followed by the Tukey's test for multiple comparisons was used. The cumulative probability of survival based on volume (2000 $mm^3$) were estimated in each group with a Kaplan-Meier survival curve analysis, and the results were compared with use of the log-rank test. A $p$-value of $< 0.05$ was considered statistically significant.

## Results

### *In vitro* characterization of MOC cell lines

As defined by SDS-PAGE, the band of anti-CD44-IR700 was almost the same molecular weight and fluorescence intensity as the non-conjugated control mAb (Figure 1A). After a 6 h incubation with anti-CD44-IR700, MOC1 and MOC2-luc cells showed high fluorescence signal, which was confirmed with flow cytometry (Figure 1B and C) and fluorescence microscopy (Figure 1D). These signals were completely blocked by adding excess anti-CD44 mAb (Figure 1B and C), indicating that anti-CD44-IR700 binds specifically. The IR700 fluorescence signals of MOC2-luc cells were higher than MOC1 cells (Figure 1B, C and D).

### *In vitro* NIR-PIT

Immediately after exposure, NIR light induced cellular swelling, bleb formation, and rupture of vesicles representing necrotic cell death (Video S1 and S2). Most of these morphologic changes were observed within 15 min of light exposure (Figure 1D), indicating rapid induction of necrotic cell death. Based on incorporation of PI, percentage of cell death increased in a light dose dependent manner (Figure 1E and F). There was no significant cytotoxicity associated with IR700 dye alone with NIR light, with NIR light alone in the absence of APC and with APC alone without NIR light. Percentage cell death in MOC2-luc cells was higher than in MOC1 cells at the same light doses. For instance, when exposed to 4J of NIR light the percentage of cell death in MOC2-luc cells was over 80% (Figure 1F), while it was less than 60% in MOC1 cells (Figure 1E). Bioluminescence showed a decrease of luciferase activity in a light dose dependent manner and in relative luciferase activity (Figure 1G) in MOC2-luc cells (Figure 1H).

### *In vivo* fluorescence imaging studies

Moderate fluorescence intensity from anti-CD44-IR700 was observed in MOC1 with high fluorescence intensity seen in MOC2 tumors 1 day after APC injection after which the fluorescence in both cell types gradually decreased (Figure 2A and B). Similarly, the target-to-background ratio (TBR) of anti-CD44-IR700 in both tumors was high 24h after APC injection, following which the TBR decreased over the following days (Figure 2C). The highest TBR was observed one day after APC injection.

### *In vivo* NIR-PIT for MOC1 tumor in a unilateral tumor model

The NIR-PIT regimen and imaging protocol are depicted in Figure 3A. One day after injection of anti-CD44-IR700, the tumors were exposed to 50 J/cm$^2$ of NIR light. IR700 tumor fluorescence signal decreased due to dispersion of fluorophore from dying cells and partial photo-bleaching, while in the absence of NIR light, the IR700 fluorescence gradually decreased over the following days (Figure 3B). Tumor growth was significantly inhibited in the NIR-PIT treatment group compared with the other groups ($p < 0.001$) (Figure 3C), and significantly prolonged survival was achieved in the NIR-PIT group ($p < 0.001$ vs. other groups) (Figure 3D). No significant therapeutic effect was observed in the other groups. There was no skin necrosis or toxicity attributable to the APC in any group.

Almost all fluorescence disappeared 24 h after 100 J/cm$^2$ of NIR-PIT (Figure 4B). Hematoxylin and eosin (H&E) staining of NIR-PIT treated MOC1 tumors revealed diffuse necrosis and micro-hemorrhage, with scattered clusters of live but damaged tumor cells, while no obvious damage was observed in the tumor receiving only anti-CD44-IR700 but no light (Figure 4C).

### *In vivo* NIR-PIT for MOC1 tumor in bilateral tumors model

Local CD44-targeted NIR-PIT was performed only on right-sided tumors in mice bearing bilateral tumors. Like the unilateral model, after exposure of the right sided tumor to 100 J/cm$^2$ of NIR light, IR700 tumor fluorescence signal decreased due to dying cells and partial photo-bleaching, while the IR700 fluorescence of the untreated left-sided tumors did not change (Figure S1B). Tumor growth was significantly inhibited in the treated tumors

compared with the other tumors ($p < 0.001$ vs. control tumors) (Figure S1C). There were no significant differences between the two groups in survival owing to the continued growth of left sided tumors which determined survival (Figure S1D). H&E staining of NIR-PIT treated tumors revealed diffuse necrosis and micro-hemorrhage, with scattered clusters of live but damaged tumor cells (Figure S1E). On the other hand, no obvious damage was observed in control tumors including contralateral untreated left-sided tumors (Figure S1E).

### *In vivo* NIR-PIT for MOC2-luc tumor in a unilateral tumor model

The NIR-PIT regimen and imaging protocol are depicted in Figure 5A. NIR-PIT resulted in decreases in bioluminescence in the treated tumor (Figure 5B) but increases in bioluminescence in other tumor groups due to rapid tumor growth. In contrast, luciferase activity decreased 1 day and 2 day after NIR-PIT ($p < 0.05$ vs. other groups) (Figure 5C). After exposure to 50 J/cm$^2$ of NIR light, IR700 tumor fluorescence signal markedly decreased compared to tumors receiving anti-CD44-IR700 but no NIR light (Figure 5D). Tumor growth was significantly inhibited in the NIR-PIT treatment group ($p < 0.001$) (Figure 5E), and significantly prolonged survival was achieved in the NIR-PIT group ($p < 0.001$ vs. other groups) (Figure 5F). No significant therapeutic effect was observed in the control groups.

High fluorescence intensity was shown in MOC2-luc tumors 24 h after anti-CD44-IR700 injection. The IR700 fluorescence signals of MOC2-luc tumor were higher compared with the signals of MOC1 tumor (Figure 6B; MOC2-luc tumor vs. Figure 4B; MOC1 tumor). Fluorescence almost completely disappeared 24 h after 100 J/cm$^2$ of NIR-PIT (Figure 6B). H&E staining of NIR-PIT treated MOC2-luc tumors revealed diffuse necrosis and micro-hemorrhage, with scattered clusters of live but damaged tumor cells, while no obvious damage was observed in the tumor receiving only anti-CD44-IR700 but no light (Figure 6C).

### *In vivo* NIR-PIT for MOC2-luc tumor in bilateral tumors model

The treatment and imaging regimen is shown in Figure S2A. Local CD44-targeted NIR-PIT was performed only on the right-sided tumors in mice bearing bilateral tumors. NIR-PIT resulted in decreases in bioluminescence of right-sided tumor (Figure S2B) while luciferase activity of both tumors in control group and untreated left-sided tumors of NIR-PIT group increased due to rapid tumor growth. In contrast, luciferase activity of treated right-sided tumors decreased 1 day and 2 days after NIR-PIT ($p < 0.001$ vs. other tumors for 1day, $p < 0.01$ vs. other tumors for 2 days, respectively) (Figure S2C). After exposure to 100 J/cm$^2$ of NIR light, IR700 tumor fluorescence signal of treated right-sided tumors decreased, while the IR700 fluorescence of untreated left-sided tumors slightly decreased after NIR-PIT(Figure S2D). Tumor growth was significantly inhibited in the treated right-sided tumors compared with the other tumors ($p < 0.01$ vs. untreated left-sided tumors, $p < 0.001$ vs. control tumors, respectively) (Figure S2E). Moreover, tumor growth was also significantly inhibited in the untreated left-sided tumors compared with the tumors in control group ($p < 0.05$ vs. both tumors of control group) (Figure S2E). Significantly prolonged survival was achieved in the NIR-PIT group ($p < 0.01$ vs. control group) (Figure S2F). There was no toxicity attributable to the APC in NIR-PIT group. H&E staining of NIR-PIT treated MOC2-

luc tumors revealed diffuse necrosis and micro-hemorrhage, with scattered clusters of live but damaged tumor cells (Figure S2G). On the other hand, only the tumor surface area was damaged in untreated left-sided tumors (Figure S2H).

### *In vivo* NIR-PIT for MOC2 mKate2 tumor in a unilateral tumor model

The NIR-PIT regimen and imaging protocol are depicted in Figure S3A. In IR700 fluorescence imaging, one day after injection of anti-CD44-IR700, the tumors showed higher fluorescence intensity (Figure S3B). In mKate2 fluorescence real-time imaging, the tumor treated by NIR-PIT showed decreasing mKate2 fluorescence signal (Figure S3C). Tumor growth was significantly inhibited in the NIR-PIT treatment group compared with the control group ($p < 0.001$) (Figure S3D), and significantly prolonged survival was achieved in the NIR-PIT group ($p < 0.001$ vs. control group) (Figure S3E).

### *In vivo* NIR-PIT for MOC2 mKate2 tumor in bilateral tumors model

The treatment and imaging regimen is shown in Figure S4A. Local CD44-targeted NIR-PIT was performed only on right-sided tumors in mice bearing bilateral tumors (Figure S4B). In mKate2 fluorescence real-time imaging, the tumor treated by NIR-PIT showed decreasing mKate2 fluorescence signal, while the mKate2 fluorescence of control tumors including untreated left-sided tumors did not change (Figure S4C). Tumor growth was significantly inhibited in the treated right-sided tumors ($p < 0.001$ vs. other control tumors) (Figure S4D). Moreover, tumor growth was also significantly inhibited in the untreated left-sided tumors compared with the tumors in control group ($p < 0.05$ vs. both tumors of control group) (Figure S4D). Significantly prolonged survival was achieved in the NIR-PIT group ($p < 0.01$ vs. control group) (Figure S4E).

## Discussion

Near infrared photoimmunotherapy (NIR-PIT) using anti-CD44-IR700 conjugate demonstrates efficacy in treating CD44-expressing syngeneic mouse models of OSCC (Figure 3–6 and Figure S1–S4). NIR-PIT with anti-CD44-IR700 led to rapid cell death *in vitro* (Figure 1, Video S1 and S2) and tumor growth reduction with survival improvements (Figure 3, 5 and Figure S3). Importantly, in immunologic tumors such as MOC2 tumors, treatment effects could be measured in the non-irradiated tumors (Figure S2 and S4).

There are several preconditions for successful NIR-PIT. First, there must be adequate uptake and retention of the APC in the target tumor. *In vivo* fluorescence imaging clearly showed the cell lines taking up the APC (Figure 2). Thus, the conjugation of IR700 to the antibody minimally alters the pharmacokinetics of antibody.

Another pre-requisite for successful NIR-PIT is that the treatment is tumor specific to avoid side effects. The anti-CD44 antibody has demonstrated clinical activity as monotherapy, however, it is associated with significant skin toxicity, including a case of lethal epidermal necrolysis (16–18). Recently, it was reported that a first-in-human phase 1 clinical trial with a new mAb targeting the constant region of CD44 showed an acceptable safety profile in patients with advanced, CD44-expressing solid tumors, however, this study was terminated early due to modest clinical efficacy (best response was stable disease) and lack of a clinical

and/or pharmacodynamics dose-response relationship (34). NIR-PIT has several advantages because it is minimally invasive, has few side effects and can be used repeatedly (35). Moreover, the dose of the APC needed for NIR-PIT is much lower than naked antibody monotherapy doses those posing lower risks of systemic side effects.

The models used in this study are syngeneic and therefore cast light on the immunologic consequences of NIR-PIT. MOC models are carcinogen-induced, fully syngeneic on a C57BL/6 genetic background, and consist of cell lines with genetic alterations that mirror human OSCC (28, 32, 33, 36). Cells treated with NIR-PIT undergo rapid volume expansion leading to rupture of the cell membrane and extrusion of cell contents into the extracellular space (Figure 1, Video S1 and S2), also known as, an immunogenic cell death (ICD) in contrast to most other treatments that result in apoptosis (26, 37–39). After NIR-PIT signaling moieties including calreticulin, ATP, and HMGB1 effectively promote maturation of immature dendritic cells (26) which are capable of digesting the cancer cell debris. These effects were in evidence in this study as non-treated tumors showed responses and this resulted in overall prolonged survival. Looking towards the future, NIR-PIT, using antibodies targeting immune-suppressor cells could result in rapid activation of cytotoxic CD8+T- and NK-cells both locally and at other untreated sites in the body (23).

It is noteworthy that no contralateral therapeutic effect was observed in bilateral tumors models of MOC1 (Figure S1). On the other hand, MOC2-luc and MOC2 mKate2 showed a response to treatment in contralateral tumors (Figure S2 and S4). However, IR700 fluorescence signals in untreated left-sided tumors were also slightly decreased after contralateral NIR-PIT despite shielding the left sided tumors from light exposure by covering them with aluminum foil (Figure S2D and S4B). Moreover, pathological analysis of untreated left-sided tumors of the MOC2-luc revealed that cellular necrosis and micro-hemorrhage, identical in quality to the NIR-PIT treated side, were observed albeit limited to the tumor surface (Figure S2H). These results suggest the possibility that despite, shielding there was internal scattering of light within the mouse body resulting in a mild NIR-PIT effect.

NIR-PIT shows highly target-specific cytotoxicity, and NIR light can be easily delivered to lesions in the mouth, such as CD44 expressing cancers of the pharynx or larynx. On the other hand, an obvious limitation of NIR-PIT is the inability to deliver NIR light to tumors located deep to the surface. NIR light can penetrate several centimeters into tissue (40), but eventually skin, fat and other organs will absorb NIR light before it reaches deeper tumor tissue. There are several potential solutions to this problem. For instance, NIR light could be delivered to a tumor while it is exposed as for instance, during surgery. Alternatively, light could be administered endoscopically (e.g. bronchus, bowel, ureter etc.) or via needle trocars in organs. Another caveat of this study is that we performed one injection of the APC with one or two exposures of NIR light because C57BL/6 mice started to have skin pigmentation within 7 days after shaving and therefore were not suitable for the experiments as the pigmentation could result in excessive absorption of light. This objection can be overcome by fractionating the dose of APC followed by repeated light exposures (41, 42). It would be desirable to extend these studies to multiple doses of the APC and light.

## Conclusion

NIR-PIT using anti-CD44-IR700 can induce significant therapeutic responses after only a single injection of the conjugate and NIR light exposure in three CD44 expressing syngeneic mouse models of OSCC. Thus, NIR-PIT utilizing CD44 as the targeting antigen for the APC might be new treatment modality for OSCC especially after initial diagnosis or after locoregional recurrence.

## Supplementary Material

Refer to Web version on PubMed Central for supplementary material.

## Acknowledgments

This research was supported by the Intramural Research Program of the National Institutes of Health, National Cancer Institute, Center for Cancer Research (ZIA BC011513)

## Abbreviations

| | |
|---|---|
| **ANOVA** | one-way analysis of variance |
| **APC** | antibody-photo-absorber conjugate |
| **BLI** | bioluminescence imaging |
| **DIC** | differential interference contrast |
| **EGFR** | epidermal growth factor receptor |
| **FDA** | Food and Drug Administration |
| **H&E** | hematoxylin and eosin |
| **ICD** | immunogenic cell death |
| **IR700** | IRDye700DX |
| **LED** | light-emitting diode |
| **mAb** | monoclonal antibodies |
| **NIR** | near infrared |
| **MOC** | murine oral cancer; near-infrared |
| **OCT** | optimal cutting temperature |
| **OSCC** | oral cavity squamous cell carcinoma |
| **PBS** | phosphate buffered saline |
| **PI** | propidium iodide |
| **PIT** | photoimmunotherapy |

| | |
|---|---|
| **ROI** | regions of interest |
| **SD** | stable disease |
| **SDS-PAGE** | sodium dodecyl sulfate-polyacrylamide gel electrophoresis |
| **SEM** | standard error of the mean |
| **TBR** | target-to-background ratio |

## References


1. Kademani D. Oral cancer. Mayo Clin Proc. 2007; 82:878–87. [PubMed: 17605971]
2. Haddad RI, Shin DM. Recent advances in head and neck cancer. N Engl J Med. 2008; 359:1143–54. [PubMed: 18784104]
3. Rogers SN, Brown JS, Woolgar JA, Lowe D, Magennis P, Shaw RJ, et al. Survival following primary surgery for oral cancer. Oral Oncol. 2009; 45:201–11. [PubMed: 18674959]
4. Jamieson CH, Ailles LE, Dylla SJ, Muijtjens M, Jones C, Zehnder JL, et al. Granulocyte-macrophage progenitors as candidate leukemic stem cells in blast-crisis CML. N Engl J Med. 2004; 351:657–67. [PubMed: 15306667]
5. Lee IC, Chuang CC, Wu YC. Niche Mimicking for Selection and Enrichment of Liver Cancer Stem Cells by Hyaluronic Acid-Based Multilayer Films. ACS Appl Mater Interfaces. 2015; 7:22188–95. [PubMed: 26379083]
6. Ma Y, Liang D, Liu J, Axcrona K, Kvalheim G, Stokke T, et al. Prostate cancer cell lines under hypoxia exhibit greater stem-like properties. PLoS One. 2011; 6:e29170. [PubMed: 22216200]
7. Prince ME, Ailles LE. Cancer stem cells in head and neck squamous cell cancer. J Clin Oncol. 2008; 26:2871–5. [PubMed: 18539966]
8. Singh SK, Clarke ID, Terasaki M, Bonn VE, Hawkins C, Squire J, et al. Identification of a cancer stem cell in human brain tumors. Cancer Res. 2003; 63:5821–8. [PubMed: 14522905]
9. Muntimadugu E, Kumar R, Saladi S, Rafeeqi TA, Khan W. CD44 targeted chemotherapy for co-eradication of breast cancer stem cells and cancer cells using polymeric nanoparticles of salinomycin and paclitaxel. Colloids Surf B Biointerfaces. 2016; 143:532–46. [PubMed: 27045981]
10. Ponta H, Sherman L, Herrlich PA. CD44: from adhesion molecules to signalling regulators. Nat Rev Mol Cell Biol. 2003; 4:33–45. [PubMed: 12511867]
11. Tovuu LO, Imura S, Utsunomiya T, Morine Y, Ikemoto T, Arakawa Y, et al. Role of CD44 expression in non-tumor tissue on intrahepatic recurrence of hepatocellular carcinoma. Int J Clin Oncol. 2013; 18:651–6. [PubMed: 22706704]
12. Chen J, Zhou J, Lu J, Xiong H, Shi X, Gong L. Significance of CD44 expression in head and neck cancer: a systemic review and meta-analysis. BMC Cancer. 2014; 14:15. [PubMed: 24410905]
13. de Jong MC, Pramana J, van der Wal JE, Lacko M, Peutz-Kootstra CJ, de Jong JM, et al. CD44 expression predicts local recurrence after radiotherapy in larynx cancer. Clin Cancer Res. 2010; 16:5329–38. [PubMed: 20837694]
14. Motegi A, Fujii S, Zenda S, Arahira S, Tahara M, Hayashi R, et al. Impact of Expression of CD44, a Cancer Stem Cell Marker, on the Treatment Outcomes of Intensity Modulated Radiation Therapy in Patients With Oropharyngeal Squamous Cell Carcinoma. Int J Radiat Oncol Biol Phys. 2016; 94:461–8. [PubMed: 26867875]
15. Okada H, Yoshida J, Sokabe M, Wakabayashi T, Hagiwara M. Suppression of CD44 expression decreases migration and invasion of human glioma cells. Int J Cancer. 1996; 66:255–60. [PubMed: 8603821]
16. Rupp U, Schoendorf-Holland E, Eichbaum M, Schuetz F, Lauschner I, Schmidt P, et al. Safety and pharmacokinetics of bivatuzumab mertansine in patients with CD44v6-positive metastatic breast cancer: final results of a phase I study. Anticancer Drugs. 2007; 18:477–85. [PubMed: 17351401]
17. Sauter A, Kloft C, Gronau S, Bogeschdorfer F, Erhardt T, Golze W, et al. Pharmacokinetics, immunogenicity and safety of bivatuzumab mertansine, a novel CD44v6-targeting

immunoconjugate, in patients with squamous cell carcinoma of the head and neck. Int J Oncol. 2007; 30:927–35. [PubMed: 17332932]

18. Tijink BM, Buter J, de Bree R, Giaccone G, Lang MS, Staab A, et al. A phase I dose escalation study with anti-CD44v6 bivatuzumab mertansine in patients with incurable squamous cell carcinoma of the head and neck or esophagus. Clin Cancer Res. 2006; 12:6064–72. [PubMed: 17062682]
19. Mitsunaga M, Ogawa M, Kosaka N, Rosenblum LT, Choyke PL, Kobayashi H. Cancer cell-selective in vivo near infrared photoimmunotherapy targeting specific membrane molecules. Nat Med. 2011; 17:1685–91. [PubMed: 22057348]
20. Nagaya T, Nakamura Y, Sato K, Harada T, Choyke PL, Hodge JW, et al. Near infrared photoimmunotherapy with avelumab, an anti-programmed death-ligand 1 (PD-L1) antibody. Oncotarget. 2016
21. Nagaya T, Nakamura Y, Sato K, Harada T, Choyke PL, Kobayashi H. Near infrared photoimmunotherapy of B-cell lymphoma. Mol Oncol. 2016; 10:1404–14. [PubMed: 27511870]
22. Nagaya T, Nakamura Y, Sato K, Zhang YF, Ni M, Choyke PL, et al. Near infrared photoimmunotherapy with an anti-mesothelin antibody. Oncotarget. 2016; 7:23361–9. [PubMed: 26981775]
23. Sato K, Sato N, Xu B, Nakamura Y, Nagaya T, Choyke PL, et al. Spatially selective depletion of tumor-associated regulatory T cells with near-infrared photoimmunotherapy. Sci Transl Med. 2016; 8:352ra110.
24. Sato K, Watanabe R, Hanaoka H, Harada T, Nakajima T, Kim I, et al. Photoimmunotherapy: comparative effectiveness of two monoclonal antibodies targeting the epidermal growth factor receptor. Mol Oncol. 2014; 8:620–32. [PubMed: 24508062]
25. Watanabe R, Hanaoka H, Sato K, Nagaya T, Harada T, Mitsunaga M, et al. Photoimmunotherapy targeting prostate-specific membrane antigen: are antibody fragments as effective as antibodies? J Nucl Med. 2015; 56:140–4. [PubMed: 25500827]
26. Ogawa M, Tomita Y, Nakamura Y, Lee MJ, Lee S, Tomita S, et al. Immunogenic cancer cell death selectively induced by near infrared photoimmunotherapy initiates host tumor immunity. Oncotarget. 2017; 8:10425–36. [PubMed: 28060726]
27. Judd NP, Allen CT, Winkler AE, Uppaluri R. Comparative analysis of tumor-infiltrating lymphocytes in a syngeneic mouse model of oral cancer. Otolaryngol Head Neck Surg. 2012; 147:493–500. [PubMed: 22434099]
28. Moore EC, Cash HA, Caruso AM, Uppaluri R, Hodge JW, Van Waes C, et al. Enhanced Tumor Control with Combination mTOR and PD-L1 Inhibition in Syngeneic Oral Cavity Cancers. Cancer Immunol Res. 2016; 4:611–20. [PubMed: 27076449]
29. Shah S, Caruso A, Cash H, Waes CV, Allen CT. Pools of programmed death-ligand within the oral cavity tumor microenvironment: Variable alteration by targeted therapies. Head Neck. 2016; 38:1176–86. [PubMed: 27061215]
30. Shcherbo D, Merzlyak EM, Chepurnykh TV, Fradkov AF, Ermakova GV, Solovieva EA, et al. Bright far-red fluorescent protein for whole-body imaging. Nat Methods. 2007; 4:741–6. [PubMed: 17721542]
31. Shcherbo D, Murphy CS, Ermakova GV, Solovieva EA, Chepurnykh TV, Shcheglov AS, et al. Far-red fluorescent tags for protein imaging in living tissues. Biochem J. 2009; 418:567–74. [PubMed: 19143658]
32. Judd NP, Winkler AE, Murillo-Sauca O, Brotman JJ, Law JH, Lewis JS Jr, et al. ERK1/2 regulation of CD44 modulates oral cancer aggressiveness. Cancer Res. 2012; 72:365–74. [PubMed: 22086849]
33. Onken MD, Winkler AE, Kanchi KL, Chalivendra V, Law JH, Rickert CG, et al. A surprising cross-species conservation in the genomic landscape of mouse and human oral cancer identifies a transcriptional signature predicting metastatic disease. Clin Cancer Res. 2014; 20:2873–84. [PubMed: 24668645]
34. der Houven van Oordt CW, Gomez-Roca C, Herpen CV, Coveler AL, Mahalingam D, Verheul HM, et al. First-in-human phase I clinical trial of RG7356, an anti-CD44 humanized antibody, in patients with advanced, CD44-expressing solid tumors. Oncotarget. 2016

35. Wilson BC, Patterson MS. The physics, biophysics and technology of photodynamic therapy. Phys Med Biol. 2008; 53:R61–109. [PubMed: 18401068]

36. Moore E, Clavijo PE, Davis R, Cash H, Van Waes C, Kim Y, et al. Established T Cell-Inflamed Tumors Rejected after Adaptive Resistance Was Reversed by Combination STING Activation and PD-1 Pathway Blockade. Cancer Immunol Res. 2016; 4:1061–71. [PubMed: 27821498]

37. Kerr JF. Shrinkage necrosis: a distinct mode of cellular death. J Pathol. 1971; 105:13–20. [PubMed: 4108566]

38. Willingham MC. Cytochemical methods for the detection of apoptosis. J Histochem Cytochem. 1999; 47:1101–10. [PubMed: 10449530]

39. Ziegler U, Groscurth P. Morphological features of cell death. News Physiol Sci. 2004; 19:124–8. [PubMed: 15143207]

40. Henderson TA, Morries LD. Near-infrared photonic energy penetration: can infrared phototherapy effectively reach the human brain? Neuropsychiatr Dis Treat. 2015; 11:2191–208. [PubMed: 26346298]

41. Mitsunaga M, Nakajima T, Sano K, Choyke PL, Kobayashi H. Near-infrared theranostic photoimmunotherapy (PIT): repeated exposure of light enhances the effect of immunoconjugate. Bioconjug Chem. 2012; 23:604–9. [PubMed: 22369484]

42. Nagaya T, Sato K, Harada T, Nakamura Y, Choyke PL, Kobayashi H. Near Infrared Photoimmunotherapy Targeting EGFR Positive Triple Negative Breast Cancer: Optimizing the Conjugate-Light Regimen. PLoS One. 2015; 10:e0136829. [PubMed: 26313651]

**Implications**

This study using syngeneic mouse models, which better model the disease in humans than conventional xenografts, suggests that NIR-PIT with anti-CD44-IR700 is a potential candidate for the treatment of OSCC.

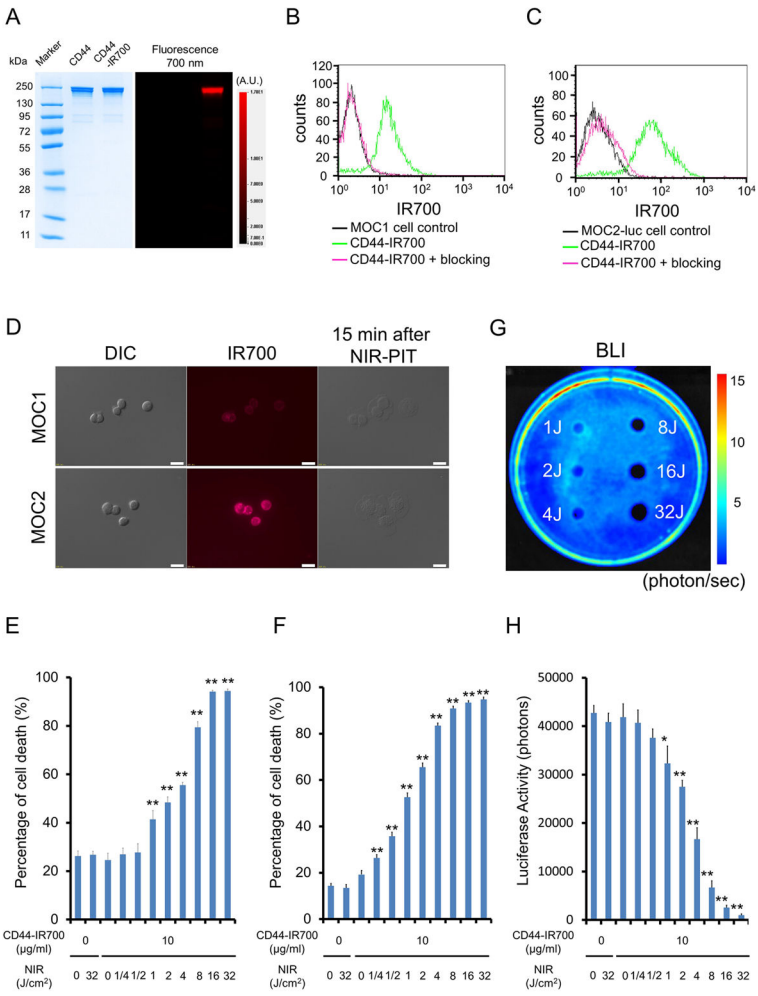


**Figure 1. Confirmation of CD44 expression as a target for NIR-PIT in MOC cells, and evaluation of *in vitro* NIR-PIT**

(A) Validation of anti-CD44-IR700 by SDS-PAGE (left: Colloidal Blue staining, right: IR700 fluorescence). Diluted anti-CD44 antibody was used as a control. (B) Expression of CD44 in MOC1 cells was examined with FACS. After 6 h of anti-CD44-IR700 incubation, MOC1 cells showed high fluorescence signal. (C) Expression of CD44 in MOC2 cells was examined with FACS. After 6 h of anti-CD44-IR700 incubation, MOC2 cells showed high fluorescence signal. (D) Differential interference contrast (DIC) and fluorescence microscopy images of MOC1 and MOC2 cells after incubation with anti-CD44-IR700 for 6 h. Moderate IR700 fluorescence signal was shown in MOC1 cells and higher IR700 fluorescence signal was shown in MOC2-luc cells. Necrotic cell death was observed upon excitation with NIR light (after 15min) in both cells. Scale bars = 20 μm. (E) Membrane damage of MOC1 cells induced by NIR-PIT was measured with the dead cell count using propidium iodide (PI) staining, which increased in a light dose dependent manner (n = 5, $^{**}p < 0.01$, vs. untreated control, by Student's t test). (F) PI staining showed membrane damage of MOC2-luc cells (n = 5, $^{**}p < 0.01$, vs. untreated control, by Student's t test). (G) Bioluminescence imaging (BLI) of a 10 cm dish demonstrated that luciferase activity in MOC2-luc cells decreased in a NIR-light dose-dependent manner. (H) Luciferase activity in

MOC2-luc cells was measured, which also decreased in a NIR-light dose-dependent manner (n = 5, $^{*}p < 0.05$ vs. untreated control, $^{**}p < 0.01$ vs. untreated control, by Student's t test).

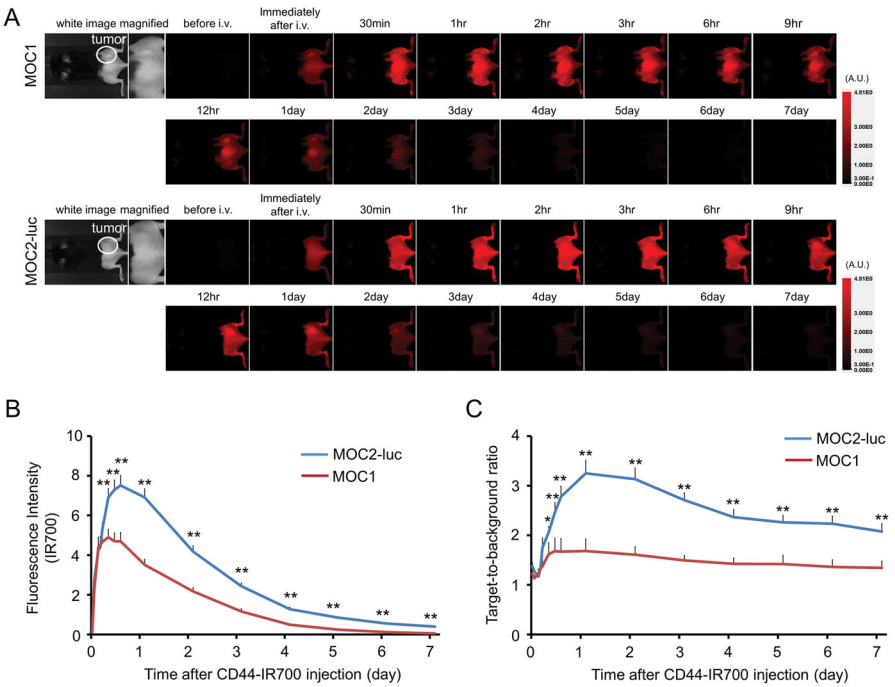


**Figure 2. *In vivo* IR700 fluorescence imaging of MOC1 and MOC2-luc tumor**

(A) *In vivo* anti-CD44-IR700 fluorescence real-time imaging of tumor-bearing mice (right dorsum). The tumor showed high fluorescence intensity after injection and the intensity was gradually decreased over days. (B) Quantitative analysis of IR700 intensities in both tumors (n = 10). The IR700 fluorescence intensity of both tumors shows high intensities within 1 day after APC injection but this decreased gradually over days. The overall IR700 intensity over time was significantly higher in MOC2-luc tumors compared with MOC1 tumors at most time points ($^{**}p < 0.01$, by Mann-Whitney test). (C) Quantitative analysis of TBR in both tumors (n = 10). TBR was high 1 day after APC injection, following which the TBR gradually decreased over the following days in both tumors. TBRs of MOC2-luc tumors were significantly higher than MOC1 tumors at most time points ($^{*}p < 0.05$, $^{**}p < 0.01$, by Mann-Whitney test).

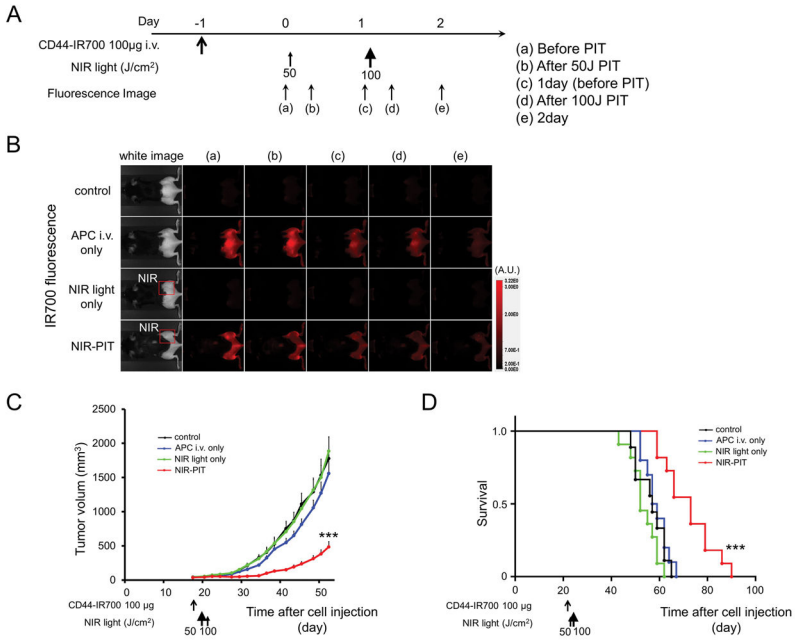


**Figure 3. *In vivo* effect of NIR-PIT for MOC1 tumor in a unilateral tumor model**

(A) NIR-PIT regimen. Fluorescence images were obtained at each time point as indicated. (B) *In vivo* IR700 fluorescence real-time imaging of tumor-bearing mice in response to NIR-PIT. The tumor treated by NIR-PIT showed decreasing IR700 fluorescence immediately after NIR-PIT. (C) Tumor growth was significantly inhibited in the NIR-PIT treatment groups (n = 10–14, ***$p < 0.001$ vs. other groups, Tukey's test with ANOVA). (D) Significantly prolonged survival was observed in the NIR-PIT treatment group (n = 10–14, ***$p < 0.001$ vs. other groups, by Log-rank test).

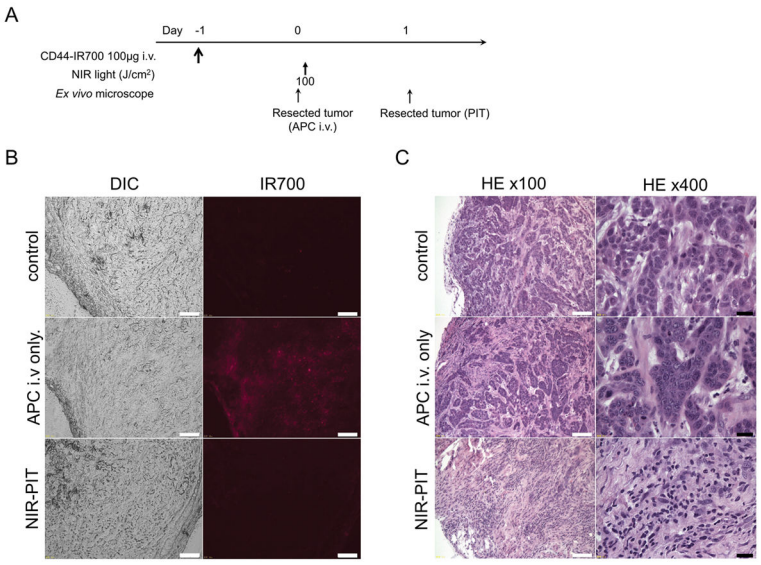


**Figure 4. *In vivo* histological fluorescence distribution and histological NIR-PIT effect for MOC1 tumor**

(A) The regimen of NIR-PIT. (B) Differential interference contrast (DIC) and fluorescence microscopy images of MOC1 tumor xenografts. Fluorescence intensity is shown in MOC1 cells 24 h after injection of anti-CD44-IR700, but the fluorescence disappears 24 h after 100 J/cm$^2$ of NIR-PIT. Scale bars = 100 μm. (C) Resected tumors were stained with H&E. A few scattered clusters of damaged tumor cells are seen within a background of diffuse cellular necrosis and micro-hemorrhage after NIR-PIT, while no obvious damage was observed after anti-CD44-IR700 alone without NIR light. White scale bars = 100 μm. Black scale bars = 20 μm.

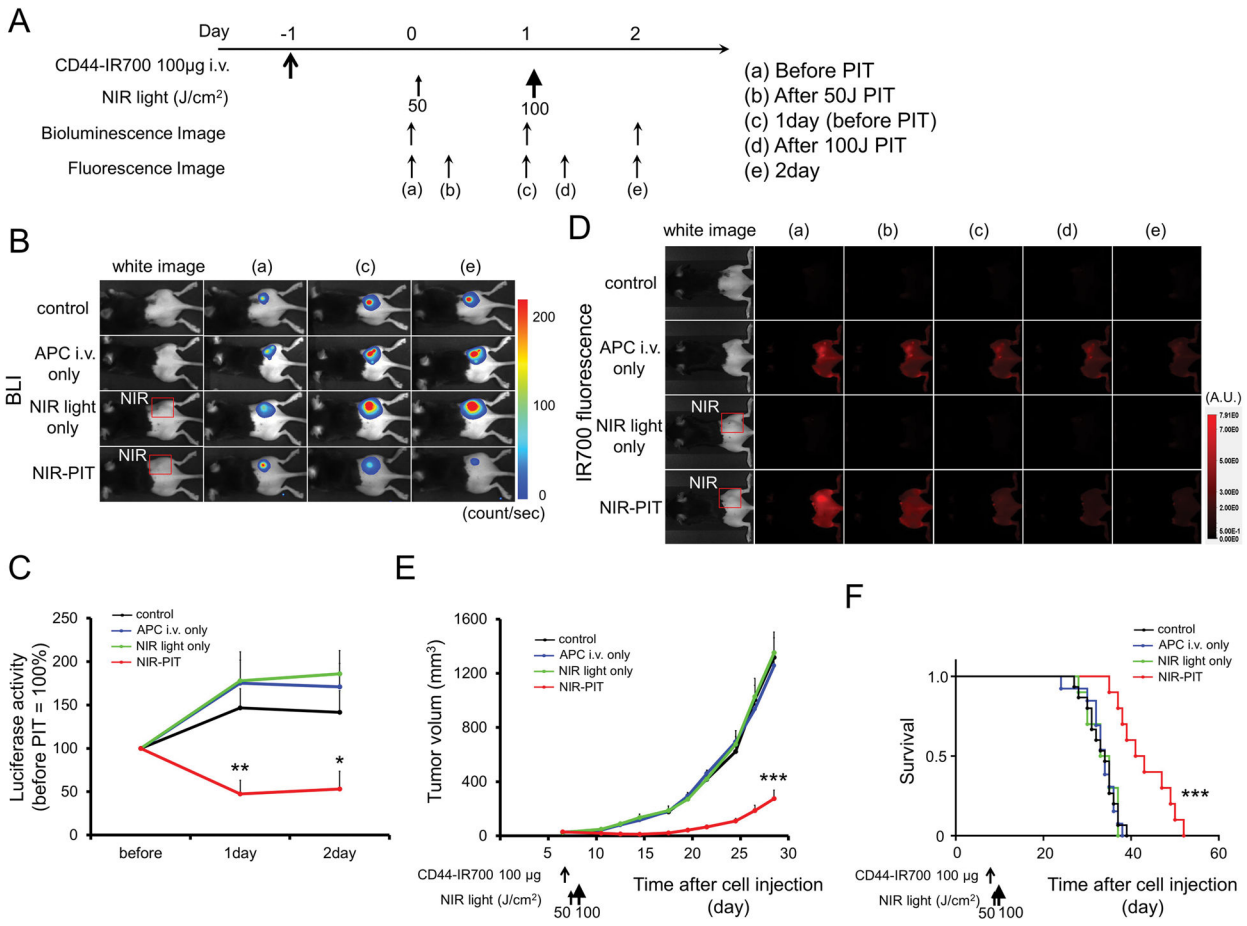


**Figure 5. *In vivo* effect of NIR-PIT for MOC2-luc tumor in a unilateral tumor model**

(A) NIR-PIT regimen. Bioluminescence and fluorescence images were obtained at each time point as indicated. (B) *In vivo* BLI of tumor bearing mice in response to NIR-PIT. Before NIR-PIT, tumors were approximately the same size and exhibited similar bioluminescence. The tumor treated by NIR-PIT showed decreasing luciferase activity after NIR-PIT. (C) Quantitative luciferase activity showed a significant decrease in NIR-PIT tumors (n ≧ 8, $^{*}p < 0.05$ vs. other groups, $^{**}p < 0.01$ vs. other groups, by Tukey's t test with ANOVA). (D) *In vivo* IR700 fluorescence real-time imaging of tumor-bearing mice in response to NIR-PIT. The tumor treated by NIR-PIT showed decreasing IR700 fluorescence immediately after NIR-PIT. (E) Tumor growth was significantly inhibited in the NIR-PIT treatment groups (n ≧ 8, ***$p < 0.001$ vs. other groups, Tukey's test with ANOVA). (F) Significantly prolonged survival was observed in the NIR-PIT treatment group (n ≧ 8, ***$p < 0.001$ vs. other groups, by Log-rank test).

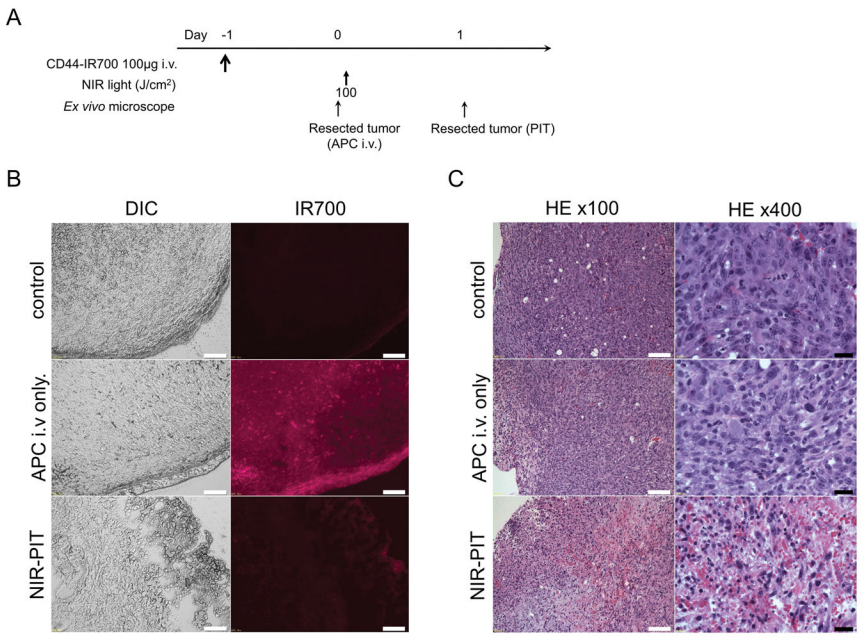


**Figure 6.** ***In vivo*** **histological fluorescence distribution and histological NIR-PIT effect for MOC2-luc tumor**

(A) The regimen of NIR-PIT. (B) Differential interference contrast (DIC) and fluorescence microscopy images of MOC2-luc tumor xenografts. Fluorescence intensity is shown in MOC2-luc cells 24 h after injection of anti-CD44-IR700, but the fluorescence disappears 24 h after 100 J/cm$^2$ of NIR-PIT. Scale bars = 100 μm. (C) Resected tumors were stained with H&E. A few scattered clusters of damaged tumor cells are seen within a background of diffuse cellular necrosis and micro-hemorrhage after NIR-PIT, while no obvious damage was observed after anti-CD44-IR700 alone without NIR light. White scale bars = 100 μm. Black scale bars = 20 μm.